Bioresource Technology 344 (2022) 126277

Contents lists available at ScienceDirect

Bioresource Technology

journal homepage: www.elsevier.com/locate/biortech

Productivity analysis in tubular photobioreactors using a dynamic photosynthesis model coupled to computational fluid dynamics particle tracking

P. Fernández del Olmo [a], F.G. Acién [b], J.M. Fernández-Sevilla [b,*]

[a] Institute for Research in Agriculture and Fisheries, Junta de Andalucía, E04720 Almería, Spain
[b] Department of Chemical Engineering, Universidad de Almería / Centre (CIESOL), Joint Centre University of Almería—CIEMAT, Ctra. Sacramento s/n, 04120 Almería, Spain

HIGHLIGHTS

- Tubular photobioreactors (TPBRs) for mass culture analyzed.
- Cell trajectories and dynamic photosynthesis model coupled to analyze productivity.
- Lomb-Scargle frequency analysis shows periodic patterns in unevenly sampled data.
- Integration factors calculated for five diameters and four circulation velocities.
- Analysis shows ample potential for improvement of current TPBRs efficiency.

GRAPHICAL ABSTRACT

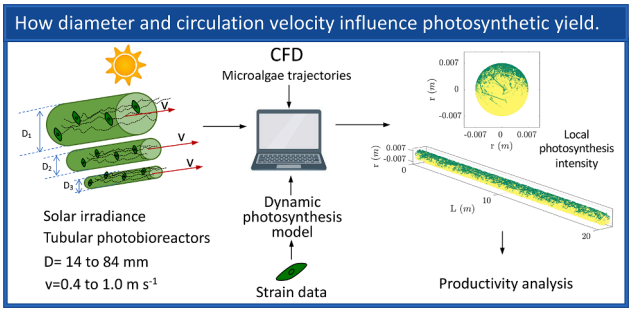

ARTICLE INFO

Keywords:
Microalgae
Light regime
Photosynthesis dynamic model
Photobioreactor
Tubular
CFD

ABSTRACT

Tubular photobioreactors (TPBRs) are closed devices used for the mass culture of microalgae. TPBRs are supposed to be well-mixed, but the influence of their specific fluid dynamics in photosynthesis efficiency has never been studied in detail. Here, we use Computational Fluid Dynamics (CFD) coupled to a dynamic photosynthesis model to analyze the efficiency of the photosynthetic response in the loop of TPBRs of different sizes (14, 24, 44, 64, and 84 mm) and circulation velocities (0.4 to 1 m s^{-1}). The results show that only the smallest diameters cause enough radial mixing for a photosynthesis-enhancing light regime (integration factor $\Gamma = 0.199$ for D = 14 mm and v = 1 m s^{-1}) while high circulation velocities in larger diameters (up to 1 m s^{-1}) increase operating costs but do not enhance photosynthetic productivity. It is also shown the relevance of the characteristic frequency of the strain (β), which is crucial for high productivity.

1. Introduction

The interest in microalgae has grown dramatically in the last two decades. During this period, microalgae have been proposed as a potential source for a wide range of products, from pharmaceuticals and nutraceuticals to additives and feed. Its application as a source of

* Corresponding author.
E-mail address: jfernand@ual.es (J.M. Fernández-Sevilla).

https://doi.org/10.1016/j.biortech.2021.126277
Received 6 September 2021; Received in revised form 29 October 2021; Accepted 30 October 2021
Available online 6 November 2021

biofuels and in wastewater treatment is also noteworthy (Chen et al., 2011; Richmond and Hu, 2013; Suparmaniam et al., 2019). The development of microalgae biotechnology and its different commercial applications have been reviewed by multiple authors (Mata et al., 2010; Spolaore et al., 2006; Wen and Chen, 2003).

While open photobioreactors, such as ponds and raceways, are economically efficient alternatives for mass production of low-value biomass or processes such as wastewater depuration, high-value applications typically require a level of quality, control, and homogeneity that can only be met by closed systems. Among these, tubular photobioreactors (TPBRs) are the most widely developed type of system and well-known technology.

Tubular PBRs are well suited for the massive cultivation of microalgae outdoors as it is a highly specialized device with a high degree of sophistication and a large illumination surface that allows obtaining good productivity (Pulz, 2001; Ugwu et al., 2008). Its main drawback is the high economic cost involved in its construction and installation. The tubular PBR design consists of two differentiated parts, namely the loop and the degasser. The loop consists of an assembly of tubes of identical diameter (generally made of PMMA) connected by means of union elements (sleeves, elbows, etc.) that provide a compact shape on a horizontal or vertical plane. The loop is specifically designed for capturing light, allowing productivity to be optimized by maximizing photosynthetic efficiency. The diameter and length of the loop and the velocity of cultivation are parameters that can be modified to supply the correct amount of light in the system. In the degasser, the exchange of heat and matter occurs, especially the desorption of O_2.

Despite all those advantages and how critical the maximization of productivity in TPBRs is for their economic feasibility, the relationship between fluid dynamics and photosynthesis is not well studied in those systems. Some aspects such as mixing and velocity distribution have been reasonably studied in tubular PBRs experimentally (Molina et al., 2001), and the availability of Computational Fluid Dynamics (CFD) has allowed a deeper, more detailed knowledge of these phenomena (Assunção and Malcata, 2020; Bitog et al., 2011; Pires et al., 2017). Still, the interplay of the fluid dynamics and the distribution of light in dense microalgal cultures in those devices, which largely impacts productivity, has been studied to a limited extent. Dark and light zones coexist inside photobioreactors because microalgal cultures are optically dense. This can be seen by comparing the average irradiance (I_{av}) and the incident or external irradiance (I_o) as proposed by Molina et al. (1997), which shows quite clearly that the light available for growth inside dense cultures is much lower than the incident. To make efficient use of the available light, the fluid dynamics in PBRs must be so that microalgal cells are cycled frequently enough between light and dark zones (Richmond, 2004). To evaluate this effectively, it is necessary to use a dynamic model of photosynthesis coupled to the fluid dynamics of the PBR (Fernández del Olmo et al., 2021).

This work presents a study on light use efficiency in tubular photobioreactors as a function of tube diameter and circulation velocity. For this, the trajectories of a statistically significant population of individual cells are traced using computational fluid dynamics (CFD), and their light history, I(t), is calculated using a light distribution model. Then, the photosynthetic performance of each case is calculated by coupling the light stories with a dynamic model of photosynthesis (Camacho Rubio et al., 2003), and these results are evaluated by comparing them to a complete light integration situation. This information allows choosing an optimal diameter for the tubular PBR loop that depends on the strain use and the specific production purpose and ascertaining to what extent increasing circulation velocity enhances the efficiency of the use of light and thus productivity. This would allow adjusting the energy consumption for pumping in TPBRs, one of the main operating costs.

2. Materials and methods

2.1. CFD model development and validation.

This work is focused on the study of fluid dynamics in tubular photobioreactors. Specifically, we have considered a 20 m straight section as bends and turns are only a small part of the volume of TPBRs and are frequently opaque. A variety of tubular PBRs sizes (inner standard commercial diameters D = 14, 24, 44, 64 and 84 mm) circulation velocities (v = 0.4, 0.6, 0.8 and 1 m s^{-1}) have been considered.

To carry out the CFD calculations, the physical space of the simulated TPBRs (computational domain) must be defined by a set of spatial cells (mesh) in a process defined as discretization. For this, the tool ANSYS Meshing 12.1 has been used. A structured hexahedral grid resulted to be the most suitable discretization of the computational domain rendering the highest quality for the available computing power.

A grid-sensitivity analysis was performed for a 20 m pipe length with the SST k-ω turbulence model. For this, five mesh densities were evaluated 1825730, 2508564, 3199392, 4479552, and 6,599,340 cells. The mesh with 3,199,392 cells was the optimal in terms of computational time and accuracy. This ensures mesh-independent results, minimizes the discretization errors, and reduces the computation time needed.

The equations that govern the behavior of the flow in the system are the continuity equation and the Reynolds averaged Navier–Stokes, which are respectively:

$$\frac{\partial u_i}{\partial x_j} = 0 \tag{1}$$

In Eq. (1), x_i represents the spatial position coordinates, and u_i is the Cartesian velocity component.

$$\frac{\partial u_i u_j}{\partial x_j} = \frac{-1}{\rho}\frac{\partial p}{\partial x_i} + \frac{\partial}{\partial x_j}\left(\nu S_{ij} - \overline{u_i' u_j'}\right) \tag{2}$$

Here, S_{ij} is the main strain rate that is calculated by:

$$S_{ij} = \frac{1}{2}\left(\frac{\partial u_i}{\partial x_j} + \frac{\partial u_j}{\partial x_i}\right) \tag{3}$$

where $\overline{u_i' u_j'} = \tau_{ij}$ is the Reynolds-stress tensor. Here, u_i' stands for the velocity fluctuation in i-direction. This set of equations is not enough because a turbulence model is also needed to model the Reynolds-stress tensor.

To determine the most appropriate turbulence model for this study, a comparative analysis was carried out between the RANS turbulence models commonly used in turbulent flow in cylindric pipes (Standard k-ε model, RNG k- ε model, k-ω SST model, and RSM) and the data obtained by Veenman (2004) (also published by Walpot et al. (2007)) using the DNS technique for two Reynolds numbers based on the bulk velocity (Re_b = 5300 and Re_b = 10300). The scheme and mesh density selected after the sensitivity analysis already commented were used to carry out the pertinent simulations. In selecting the turbulence model, the consumption of computational resources of each of the evaluated models was also considered. As can be seen in Fig. 1, where the results of normalized turbulent kinetic energy production (a) and (b) and mean axial velocity (c) are shown, the turbulence model that presented the best agreement with the data of Veenman (2004) was the SST k-ω model, which provided the best compromise between accuracy and calculation time. Therefore, this was the turbulence model chosen to simulate all the cases studied.

ANSYS FLUENT 12.1 has been used to solve the transport equations. The mathematical procedure (the Semi-Implicit Method for Pressure-Linked Equation SIMPLE routine) Patankar (1980), and the convergence criterion are described elsewhere (Fernández del Olmo et al., 2021). The transport equations are discretized using second-order upwind scheme options.

The validation of the CFD model was carried out by comparing the

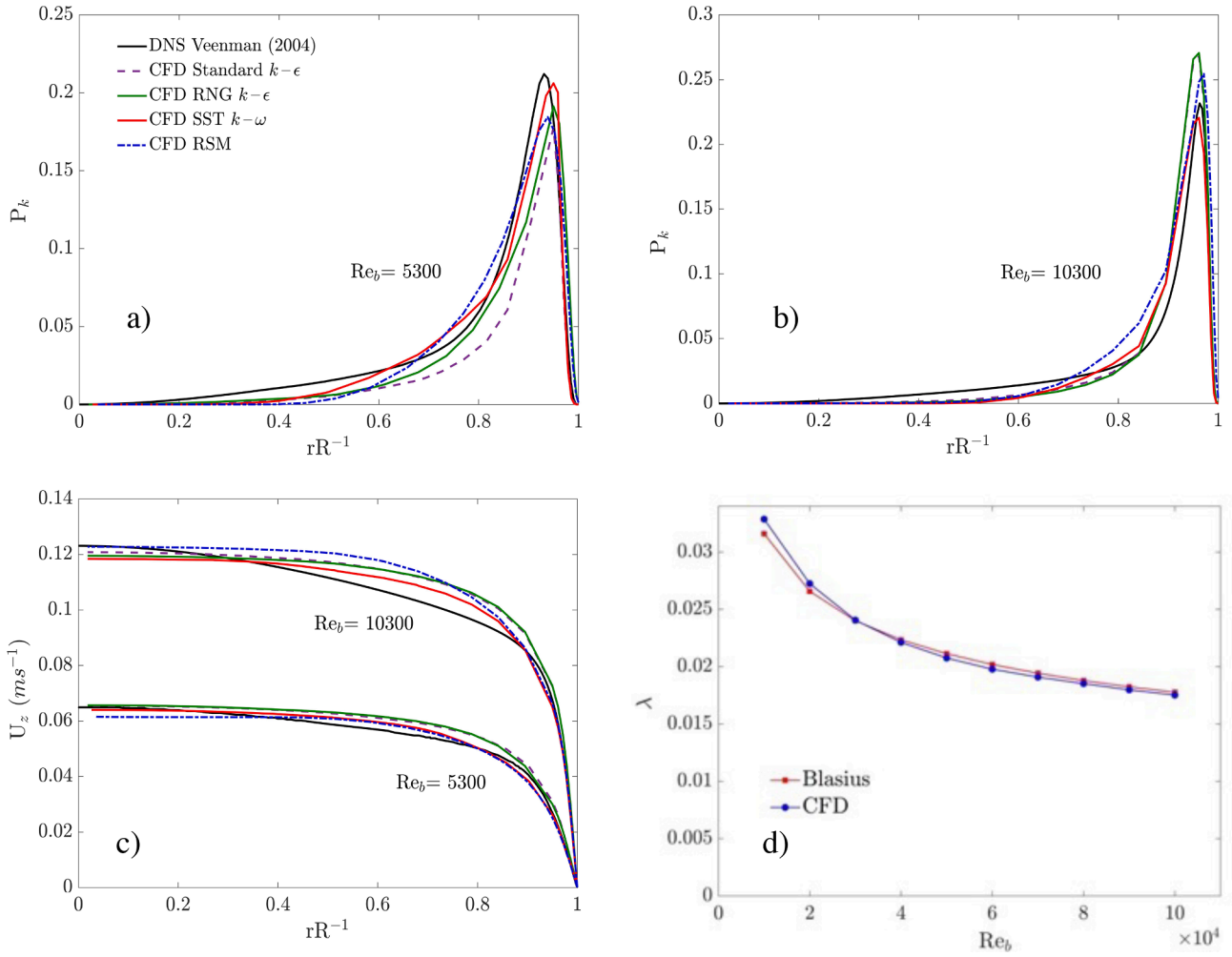

Fig. 1. Validation of the CFD model. Production of turbulent kinetic energy at a) R_{eb} = 5300 and b) R_{eb} = 10300, c) mean axial velocity profile for R_{eb} = 5300 and R_{eb} = 10300 and d) Friction factor (λ) in tubular PBR for different Reynolds numbers.

friction factor value (λ) obtained in each simulation with the one calculated using the Blasius equation (Blasius, 1913), considering different Reynolds numbers (from 10,000 to 100,000) in a pipe with an inner diameter D = 0.084 m and length L = 20 m.

The Blasius empirical correlation can be used for turbulent flow in smooth pipes (the roughness of inner tube surface covered with laminar sublayer), which is valid for 4000 ≤ Re ≤ 100000:

$$\lambda = \frac{0.3164}{\mathrm{Re}^{0.25}} \tag{4}$$

In Fig. 1.d, it can be seen that the CFD data showed a good agreement with the Blasius equation. The deviation between the friction factor obtained in the CFD simulations to that calculated using the Blasius equation was only 2.1%.

2.2. Individual cell trajectories.

A total of 50 cell trajectories inside the tubular PBR were calculated using the ANSYS FLUENT Discrete Random Walk Model (DRW) with the properties of the microalgal cells as described elsewhere (Fernández del Olmo et al., 2021).

In a DRW model, each eddy is characterized by a Gaussian-distributed random velocity fluctuation of components $u^{'}$, $v^{'}$, and $w^{'}$ and a time scale, τ_e. These are calculated as averages:

$$u^{'} = \zeta\sqrt{\overline{u'^2}} \tag{5}$$

where ζ is a normally distributed random number, and the remainder of the right-hand side is the local RMS value of the velocity fluctuations. Assuming isotropy, the following holds for SST k-ω model components:

$$\sqrt{\overline{u'^2}} = \sqrt{\overline{v'^2}} = \sqrt{\overline{w'^2}} = \sqrt{\frac{2k}{3}} \tag{6}$$

The characteristic lifetime of the eddy is defined as $\tau_e = 2T_L$. For small "tracer'' particles that move with the fluid (zero drift velocity) T_L is given by:

$$T_L = C_L\frac{k}{\epsilon} \tag{7}$$

This can be approximated for the SST k-ω model as

$$T_L \approx 0.15\frac{k}{\epsilon}$$

2.3. Frequency analysis and data processing

A Lomb-Scargle signal analysis has been used to carry out a quantitative analysis of the simulated particle trajectories as described in detail in Fernández del Olmo et al. (2021).

The Fast Fourier Transform (FFT) has been widely used before for this purpose (Gómez-Pérez et al., 2017, 2015; Perner-Nochta and Posten, 2007), but the FFT algorithm requires evenly sampled data to obtain the spectrum for the data. However, the data obtained in the

simulations on the position of each particle are unevenly spaced time.

The fundamental equation for the Lomb-Scargle Periodogram (Lomb, 1976) is:

$$P_N(\omega) \equiv \frac{1}{2\sigma^2}\left\{\frac{\left[\sum_N\left(h_n-\overline{h}\right)cos\omega(t_n-\tau)\right]^2}{\sum_N cos^2\omega(t_n-\tau)}+\frac{\left[\sum_N\left(h_n-\overline{h}\right)sin\omega(t_n-\tau)\right]^2}{\sum_N sin^2\omega(t_n-\tau)}\right\} \tag{8}$$

where the N data points are unevenly sampled events at times t_i arranged as

$h_i \equiv h(t_i), i = 0, \cdots, N-1$. The mean $\left(\overline{h}\right)$ and variance (σ^2) are calculated as

$$\overline{h} \equiv \frac{1}{N}\sum_{i=0}^{N-1} h_i \tag{9}$$

$$\sigma^2 \equiv \frac{1}{N-1}\sum_{i=0}^{N-1}\left(h_i-\overline{h}\right)^2 \tag{10}$$

$$tan(2\omega\tau) = \frac{\sum_j sin2\omega\tau_j}{\sum_j cos2\omega\tau_j} \tag{11}$$

All the calculations and data processing have been done using MATLAB (R2017a). This software was used to obtain the above-described periodograms, obtain the light history, I(t), of the simulated trajectories, and calculate the photosynthetic response by integrating the Camacho-Rubio model (Camacho Rubio et al., 2003). All these calculations are described in detail elsewhere (Fernández del Olmo et al., 2021).

2.4. Evaluation of photosynthetic efficiency

In a dense culture of microalgae, intense light gradients take place, and the trajectories of the cells, as they are carried by the fluid, influence the efficiency of photosynthesis (Brindley et al., 2011). This can be quantified by using dynamic photosynthesis models (Eilers and Peeters, 1988, Camacho Rubio et al., 2003). These models postulate that light is captured by the so-called "photosynthetic units" (PSUs) that get excited and drive photosynthesis as becoming deactivated during this process. Both models are similar (Fernández del Olmo et al., 2021) but we use Camacho Rubio et al. (2003) because we have more parameter data available. The main equations of this model are the deactivation of excited PSUs:

$$r = \frac{r_m^* \cdot a^*}{K_s^* + a^*} \tag{12}$$

The model proposed by Camacho Rubio et al. (2003) encompasses the Eilers-Peeters model because Eq. (12) can show linearity between the specific deactivation rate (r) and the concentration of excited centers (represented by a* in the Camacho-Rubio model) is much smaller than the saturation constant of the enzymatic step ($Ks^* \gg a^*$) as well as a saturation behavior typical of enzymatic reactions for larger concentrations a* ($Ks^* \ll a^*$).

$$\frac{da^*}{dt} = k_a \cdot I \cdot (a - a^*) - \frac{r_m^* \cdot a^*}{K_s^* + a^*} \tag{13}$$

where a is the concentration of PSUs (mole PSUs (g biomass)$^{-1}$) and a* is the concentration activated PSUs.

The photosynthesis rate (PO_2, mol O_2 (g biomass)$^{-1}s^{-1}$) is proportional to the deactivation rate of a*:

$$PO_2 = k \cdot \frac{r_m^* \cdot a^*}{K_s^* + a^*} \tag{14}$$

where k is the proportionality constant. The studies of (Emerson and Arnold, 1932; Nelson and Cox, 2017) on photosynthesis stoichiometry would suggest a theoretical maximum of one mole of O_2 generated per eight moles of activated centers consumed, although this proportion can vary when other deactivation mechanisms are at work.

Camacho Rubio et al. (2003) proposed a dimensionless model by dividing each parameter by the total concentration of photosynthetic centers. Thus, the concentration of activated centers (a*) becomes a fraction ($x^* = a^*/a$). In the original work, the authors organized the parameters of the model into the following groups:

$$\alpha = \frac{r_m^*}{k_a \cdot a^*};\ \beta = \frac{r_m^*}{a^*};\ \kappa = \frac{K_s^*}{a^*} \tag{15}$$

where k_a is the absorption coefficient of the photosynthetic centers. For continuous irradiance (I = constant), Eq. (13) can be integrated to (Camacho Rubio et al., 2003):

$$\frac{P_{cont}}{P_{max}} = \frac{I}{2\cdot\alpha}\cdot\left[\left(1+\kappa+\frac{\alpha}{I}\right) - \sqrt{\left(1-\kappa-\frac{\alpha}{I}\right)^2 + 4\cdot\kappa}\right] \tag{16}$$

when I_{av} is used in place of I (Molina et al., 1997), the values of P given by Eq. (16) correspond to a regimen of complete light integration. On the other hand, for a perfectly segregated light regime (local P integration), the following equation must be used:

$$\frac{P_{cont}}{P_{max}} = \frac{1}{\pi\cdot R^2}\int_{-R}^{R}\int_{-\sqrt{R^2-x}}^{\sqrt{R^2-x}} \frac{I(x,y)}{2\cdot\alpha}\cdot\left[\left(1+\kappa+\frac{\alpha}{I(x,y)}\right) - \sqrt{\left(1-\kappa-\frac{\alpha}{I(x,y)}\right)^2 + 4\cdot\kappa}\right] dydx \tag{17}$$

Where R is the tube radius, (x,y) is the position inside the tube in cartesian coordinates (x = 0, y = 0 being the center of the tube), and I(x, y) is an equation describing the light attenuation with the position inside the tube (Eq. (18)). In our case, this equation is the Lambert-Beer applied to a light beam of intensity I_o impinging perpendicularly on a cylinder, as shown in the next section.

Eqs. (14), (16), and (17) are used to obtain respectively the results of P given by the dynamic model, the equivalent continuous light response (light regime integration) and the integration of local rates. In this study, the photosynthetic response presented is the ratio P/P_{max} in order to make the results as species-independent as possible. The values chosen for the other model parameters are $\alpha = 100$ μmole photons $m^{-2}\ s^{-1}$, $\kappa = 0.1$ and $\beta = 5$ Hz as they are representative for the behavior of the most frequent strains used in microalgal mass culture (Brindley et al., 2011).

2.5. Irradiance patterns at different biomass concentration

The vertical movement of the microalgal cells inside the tubular PBR is only one of the interacting factors affecting the performance of a microalgal culture. The photosynthetic intensity of individual cells depends on the local irradiance that in a TPBR is given by the attenuation of the incident photosynthetically active radiation (PAR) I_o by the culture layer above the considered microalgae. If a Lambert-beer type attenuation is considered, the local irradiance at a given depth ×, represented as I(x), is given by the following equation

$$I(x,y) = I_o \cdot e^{-k_a \cdot C_b \cdot \left(\sqrt{R^2-x^2}-y\right)} \quad (18)$$

where k_a is the extinction coefficient of the microalgae (Molina Grima et al., 1994) that represents the intensity with which a given strain of microalgae absorbs PAR light, C_b is the biomass concentration in the culture, and (x,y) is the position inside the tube described above. The calculation in Eq. (18) assumes that I_o impinges perpendicularly on the culture surface and ignores wall effects but is otherwise representative of the actual attenuation of light in a generic microalgal culture.

To enable fair comparisons of photosynthetic activity among the different tube diameters, the biomass concentration used in each case was adjusted to attain the same light availability quantified as I_{av}. In a cylindrical system, I_{av} is calculated from its definition using the following equation:

$$I_{av} = \frac{I_o}{\pi \cdot R^2} \int_{-R}^{R} \int_{-\sqrt{R^2-x}}^{\sqrt{R^2-x}} e^{-k_a \cdot C_b \cdot \left(\sqrt{R^2-x^2}-y\right)} dy dx \quad (19)$$

Molina et al. (1997) propose a simplified equation to calculate I_{av} in tubular PBRs:

$$I_{av} = \frac{I_o}{k_a \cdot C_b \cdot 1.6 \cdot R}\left(1 - e^{-k_a \cdot C_b \cdot 1.6 \cdot R}\right) \quad (20)$$

The average irradiances chosen and the corresponding biomass concentration for each tube diameter studied are shown in Table 1.

The units of I_{av} are in μmole photons m^{-2} s^{-1}. The calculations are done for a generic attenuation coefficient of $k_a = 0.1$ m^2 $g^{-1,}$ and thus the concentration C_b is expressed in g m^{-3}.

3. Results and discussion

Mass culture of microalgal biomass in industrial photobioreactors requires a high biomass concentration and optically dense cultures capable of absorbing a high proportion of the impinging light. Therefore, PBRs naturally work with sharp light gradients, usually under sunlight. This causes over-saturating and dark zones to coexist, giving rise to the risk of simultaneously having over-saturating or even photoinhibiting zones and respiration zones, which can potentially cause a marked loss of photosynthetic efficiency and a severe decrease in productivity if not managed properly. The solution to this situation is to provide enough mixing (Richmond, 2004) so that a frequent turnover of the cells between dark and light zones allows for the microalgae population to "see" an average irradiance (I_{av}). This is more productive than a situation where microalgae move so slowly that their growth rate is adapted to the local irradiance (Brindley et al., 2016, 2011), especially in tubular PBRs. The well-mixed situation is widely known as "light integration" while the contrary is "local growth integration".

Light regime was defined by Richmond (Richmond, 2004), who showed experimentally that there is an "optimal cell density" and mixing intensity needed to maximize productivity. However, the experimental method is proposed by Richmond is impractical for industrial-size PBRs.

Table 1
Biomass concentrations (C_b, g m^{-3}) chosen to keep the light availability at the same value (as average irradiance, I_{av}) across all of the pipe diameters tested. Calculations have been done for an incident irradiance $I_o = 2000$ μmol m^{-2} s^{-1} and absorption coefficient $k_a = 0.08$ m^2 g^{-1} using the equation proposed by Molina et al. (1997) for cylindrical systems.

	Diameter (m)			
I_{av} (μmol m^{-2} s^{-1})	0.014	0.024	0.044	0.084
260	6750	3938	2138	1124
200	9000	5250	2850	1500
130	13,500	7875	4275	2250
100	18,000	10,500	5700	3000
80	22,500	13,125	7125	3750

In this regard, Fernández del Olmo et al. (2021) proposed an analysis of a raceway PBR analogous to Richmond's by coupling a dynamic photosynthesis model with the light stories I(t) of a microalgal cell population calculated by CFD.

The present work describes the optimization of the light regime in TPBRs by coupling the Camacho-Rubio dynamic photosynthesis model (Camacho Rubio et al., 2003) and CFD particle tracking. Three elements interact to produce the global photosynthetic response: the movement of the microalgal cells inside the photobioreactor, the light distribution and the growth characteristics of the particular microalgal strain being cultured represented by a dynamic growth model. These three aspects are analyzed next.

3.1. Cell trajectories

Several authors have shown that CFD is an effective tool to describe the fluid dynamics of PBRs (Gao et al., 2017; Nikolaou et al., 2016; Perner-Nochta and Posten, 2007; Prussi et al., 2014), but it is necessary to highlight that the CFD tracking of individual trajectories and position sampling needs to be done taking into account the characteristics of the photosynthetic response. The gradual shift of microalgae from "local growth integration" to "light integration" happens for irradiance fluctuations between 1 and 50 Hz (Camacho Rubio et al., 2003; Phillips and Myers, 1954; Terry, 1986). When doing CFD simulations, it is essential that the movement analyzed represents the whole PBR volume. For this reason, a representative population must be studied. In Fig. 2 are shown the trajectories of 10 particles at four circulation velocities, 0.4, 0.6, 0.8, and 1.0 m s^{-1} for diameters D = 14, 24, 44, and 84 mm; (diameter 64 mm has been omitted for clarity).

It is generally assumed that fluids circulating in turbulent conditions through pipes are radially well mixed. The observation of Reynolds experiments shows that in fully developed turbulent flow, a complete radial mixing of the dye takes place in a time that is an order of magnitude lower than one second. This would lead to the idea that the fluid elements in such conditions move from the center to the surface of the pipe several times per second and thus that microalgal cultures in tubular photobioreactors must be close to "light integration conditions". However, this is not necessarily true for microalgal cells as they are particles of a diameter well above the molecular size.

As Fig. 2 shows, microalgae frequently move from the surface to the center for all the diameters and velocities tested, but most often, the movement from surface to center is not complete, and the trajectories change midway, leading to complex patterns that invalidate the simplifications done by other authors that interpret the light regime as light/dark transitions. Additionally, Fig. 2 shows that the trajectories are irregular and that the frequency with which the test particles come close to the center varies during the simulated 20 m. Thus a particle moves with a complex trajectory of varying frequency and amplitude. This occurs for the ample range of diameters and circulation velocities tested in this work and highlights the need to analyze complete trajectories and not rely on average values of frequency and amplitude.

From Fig. 2, it is also noteworthy that the circulation velocity apparently does not substantially influence the radial movement of the microalgae. It could be expected that increasing the circulation velocity from 0.4 to 1.0 m s^{-1} should have a noticeable impact on the turbulence, but, as Fig. 2, there is no apparent change as it is impossible to visually distinguish the plots of the same diameter at different circulation velocities in the 20 m of displacement. This agrees with the observations of Perner-Nochta and Posten (2007) and Qin and Wu (2019).

In contrast to circulation velocity, Fig. 2 shows that the tube diameter affects the mixing pattern. As can be seen, the reduction in diameter contributes to increasing the radial mixing component so that for the smaller diameter, it is relatively frequent to observe particles that go from the surface to the center, practically completing an entire "light path length". These particles would be the only ones that see a complete light/dark cycle. Still, most of the particles, even for the smaller

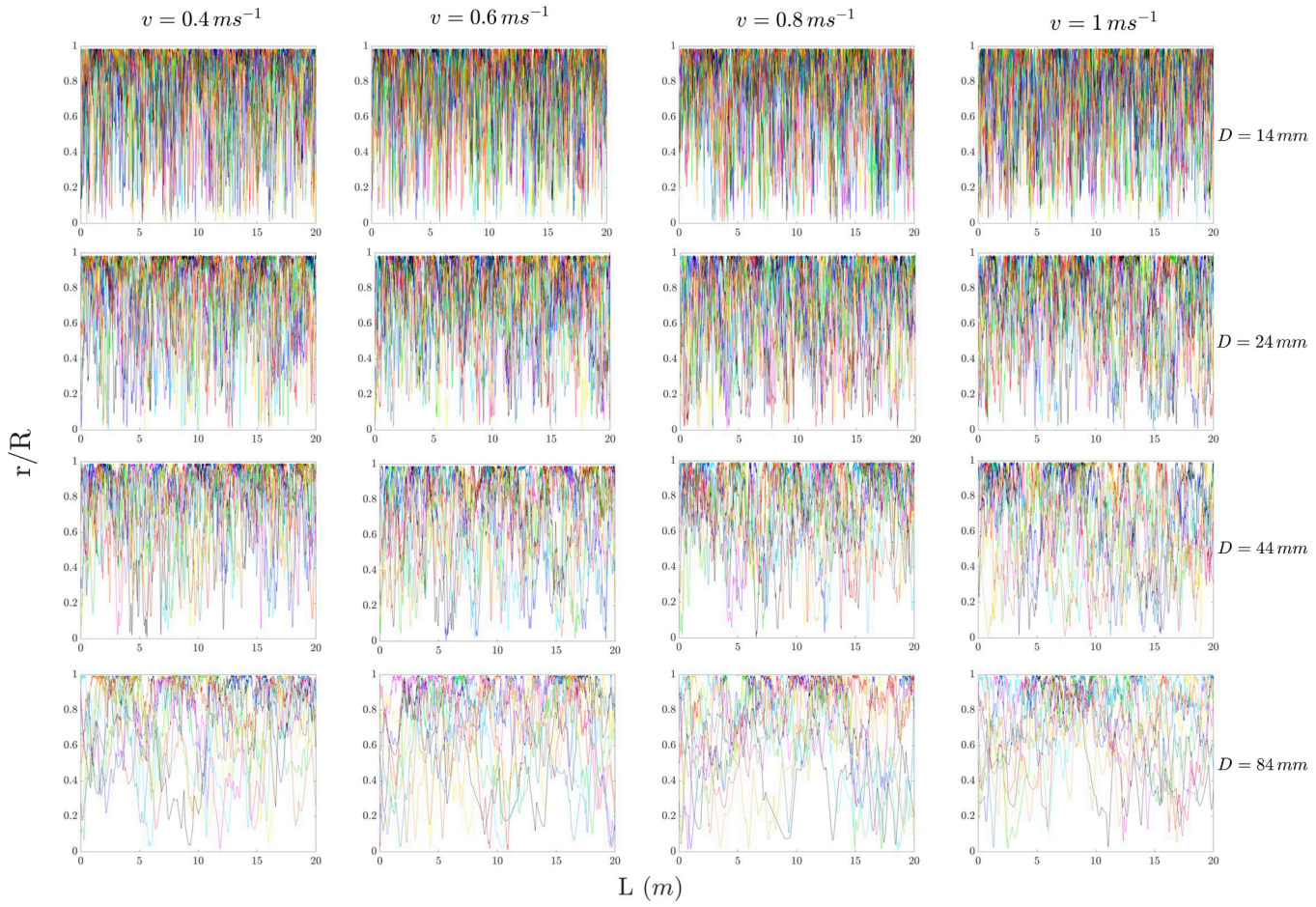

Fig. 2. Vertical movement of individual cells inside the photobioreactor at different circulation velocities (0.4, 0.6, 0.8 and 1.0 m s^{-1}). Only 10 trajectories out of 50 are shown for clarity.

diameter, do not reach the center. On the contrary, as the tube diameter increases, fewer particles reach the center, and the frequency of the light/dark transitions decreases. This is a consequence of the increased surface-to-center distance resulting in reduced productivity in the larger diameters, even if the light availability (average irradiance I_{av}) is kept constant, as described by Posten (2009).

The most relevant conclusion is the slight influence of the circulation velocity in the exposition frequency. Although it is widely accepted that a circulation velocity close to 1 m s^{-1} is desirable to enhance the turbulence, the simulations done here show that this is unnecessary with regard to light regime. This could be a factor to improve the economy of TPBRs as pumping is a relevant cost, provided that a high circulation velocity is not needed to avoid fouling or for other reasons (Belohlav et al., 2021).

Some subtle variations of the movement patterns cannot be seen in Fig. 2. Thus, a spectral analysis is carried out in section 3.3 to provide more detail.

3.2. Irradiance patterns

The movement of the microalgae inside the irradiance field I(x,y) gives rise to a population of light histories, I(t), that ultimately drive photosynthesis. This response is, thus, dependent on the biomass concentration, C_b, and should be carefully chosen so that the differences observed in the photosynthetic response can be attributed to the fluid dynamics and not to different light availability (I_{av}). The biomass concentrations for the irradiance histories shown in Fig. 3 have been selected so that the light availability, quantified as average irradiance (I_{av}), is 100 μmole photons m^{-2} s^{-1} for all of the tube diameters considered. The calculations have been done for an external irradiance corresponding to sunlight levels (I_o = 2000 μmole photons m^{-2} s^{-1}), which are the most productive conditions and the most difficult to manage, and for a generic absorption coefficient (k_a) of 0.1 m^2 g^{-1}. The average irradiance has been selected to match half the saturation constant of the Camacho-Rubio model used in this work (α = 200 μmole photons m^{-2} s^{-1}) so that the microalgae would be growing in semi-saturating conditions ($\mu=\mu_{max}/2$), which is usually the most productive situation and is particularly interesting from the point of view of this study as these conditions ensure the existence of oversaturating and dark zones.

The trajectories shown in Fig. 2 may give the impression that microalgae linger near the PBR surface a substantial part of the time and thus are most of the time receiving a high irradiance, but, as Fig. 3 shows, this is not so. In fact, only around 2% of the tube volume is receiving irradiances above 1500 μmole photons m^{-2} s^{-1}, which happens during very short times. For this reason, the trajectories in Fig. 3 rarely go near the surface and thus approach the incident irradiance I_o = 2000 μmole photons m^{-2} s^{-1}.

It can also be calculated that the proportion of volume culture above 1000 μmole photons m^{-2} s^{-1} is only around 5% for all the diameters. It is also interesting that approximately 78% is receiving an irradiance lower than the semi saturating (I < 100 μmole photons m^{-2} s^{-1} = α/2). This is the value that several authors choose to delimitate the illuminated and dark zones in the PBR and thus to determine the frequency of the transitions between light and dark zones. Another frequently chosen value to discerning between light and dark zones is the compensation

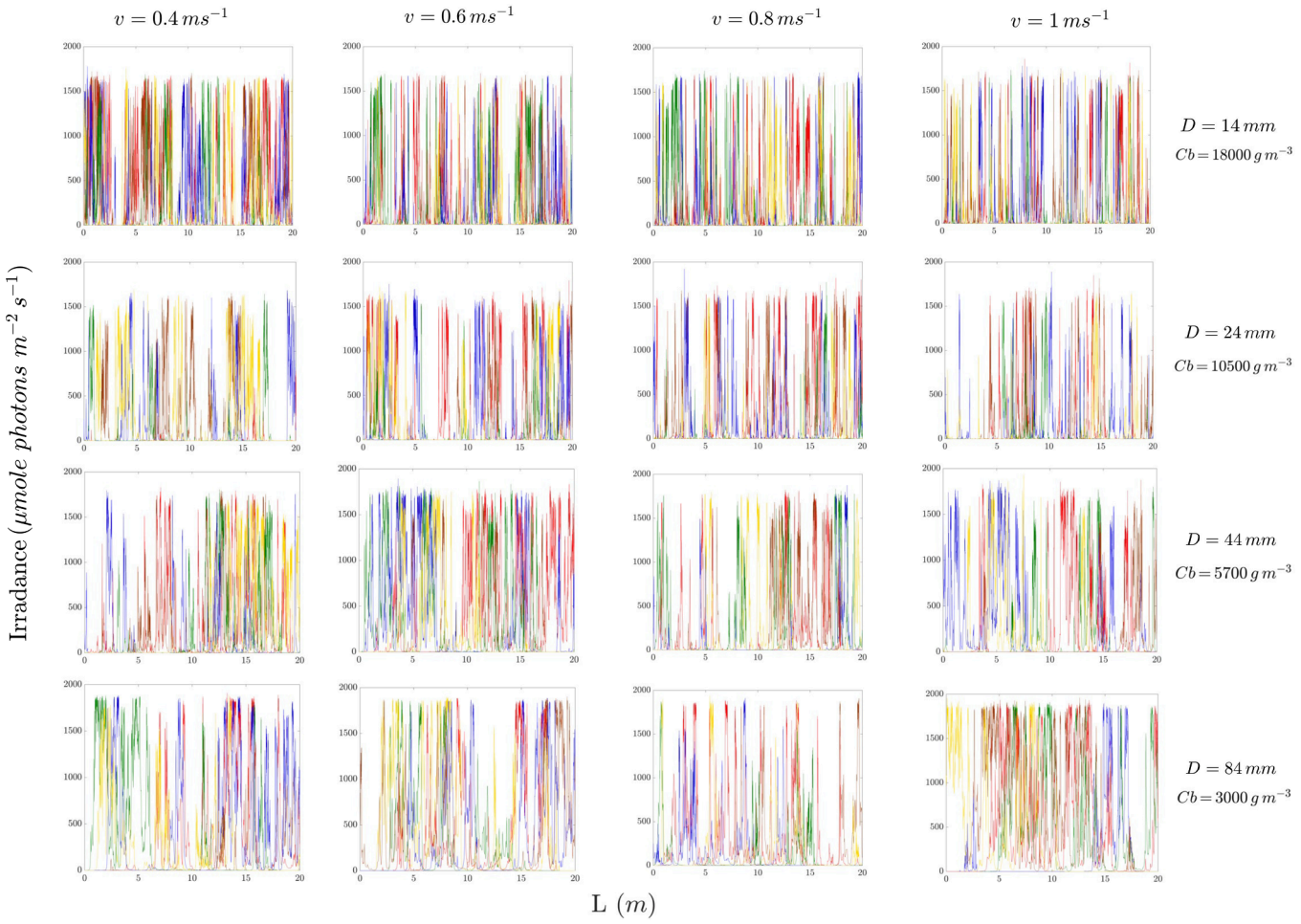

Fig. 3. Irradiance patterns, I(t) of the individual cell trajectories inside the photobioreactor at different circulation velocities (0.4, 0.6, 0.8, and 1.0 m s^{-1}) and for biomass concentrations corresponding to $I_{av} = \alpha/2 = 100$ μmole photons m^{-2} s^{-1}.Only 10 trajectories out of 50 are shown for clarity.

intensity (where $\mu_{net} = 0$) that in our case happens at 30 μmole photons m^{-2} s^{-1}. With this criterium, 30% of the volume would be considered dark, and the rest illuminated.

The data in Fig. 3 shows that, regardless of the criteria chosen to delimitate light and dark zones, the transitions are incomplete and highly irregular. The same irradiance history changes pace along the 20 m of the simulation, both in amplitude. The conclusion drawn from Fig. 3 is that representing the effect of varying light in tubular PBRs by neat dark/light transitions is futile as there are differences not only between the light histories of individual cells but a single cell can experiment repeated changes in amplitude and frequency that cannot be treated as a regular movement.

Fig. 3 also shows that the circulation velocity has minimal effect in the radial movements of the particles so that, for the same tube diameter, all four plots are virtually indistinguishable.

Concerning the influence of the tube diameter, the only observation that can be done is that individual cells "see" higher irradiances more frequently in the larger diameters. This seems counterintuitive as the light path is longer in the larger diameters, and the light attenuation should be more intense in all circumstances. However, it must be considered that Fig. 3 has been plotted with the criteria of keeping the same light availability for all the diameters, and this implies that biomass concentrations are higher for the smaller diameters and the light gradients more intense. For D = 14 mm, the biomass concentration is 18000 g $m^{-3,}$ and the consequence is that irradiance is attenuated to 1500 μmole photons m^{-2} s^{-1} only after a light path of 0.15 mm under the culture surface, while for this attenuation, the light path is 0.25, 0.45 and 0.90 mm respectively for the diameters 24, 44 and 84 mm.

On the other hand, from the data in Fig. 3, there seems to be a 0.13 mm layer close to the surface that the traced particles can difficultly penetrate. The irradiance reaching the boundary of this layer is approximately 1600, 1700, 1800, and 1900 respectively for the diameters of 14, 24, 44, and 84 mm. This apparent stationary layer corresponds to 1.8, 1.1, 0.59, and 0.31% of the total culture volume.

3.3. Spectral analysis

High photosynthetic efficiency in PBRs is attained with an adequate light regime that requires frequent transitions of the microalgal cells from dark to illuminated zones. Not only this, a significant degree of light integration only takes place when the movement of the cell is complete. This is best analyzed through the concepts of amplitude and frequency that can be obtained from data of trajectories or light history using a spectral analysis method such as the one proposed by Lomb-Scargle.

Fig. 4 shows the Lomb-Scargle periodogram obtained for the trajectories data for the same diameters and velocities in Fig. 2. The CFD data has been sampled 50 times per second, and thus the spectral analysis should be able to detect movement frequencies up to 25 Hz, but, as shown in Fig. 4, periodic movements over 3 Hz are virtually inexistent in every case. These small amplitudes correspond to displacements so small that the difference in irradiance is negligible and can be ignored.

There are two aspects to highlight from Fig. 4. First, the movement amplitude (shown as PSD) increases with the tube diameter, as the

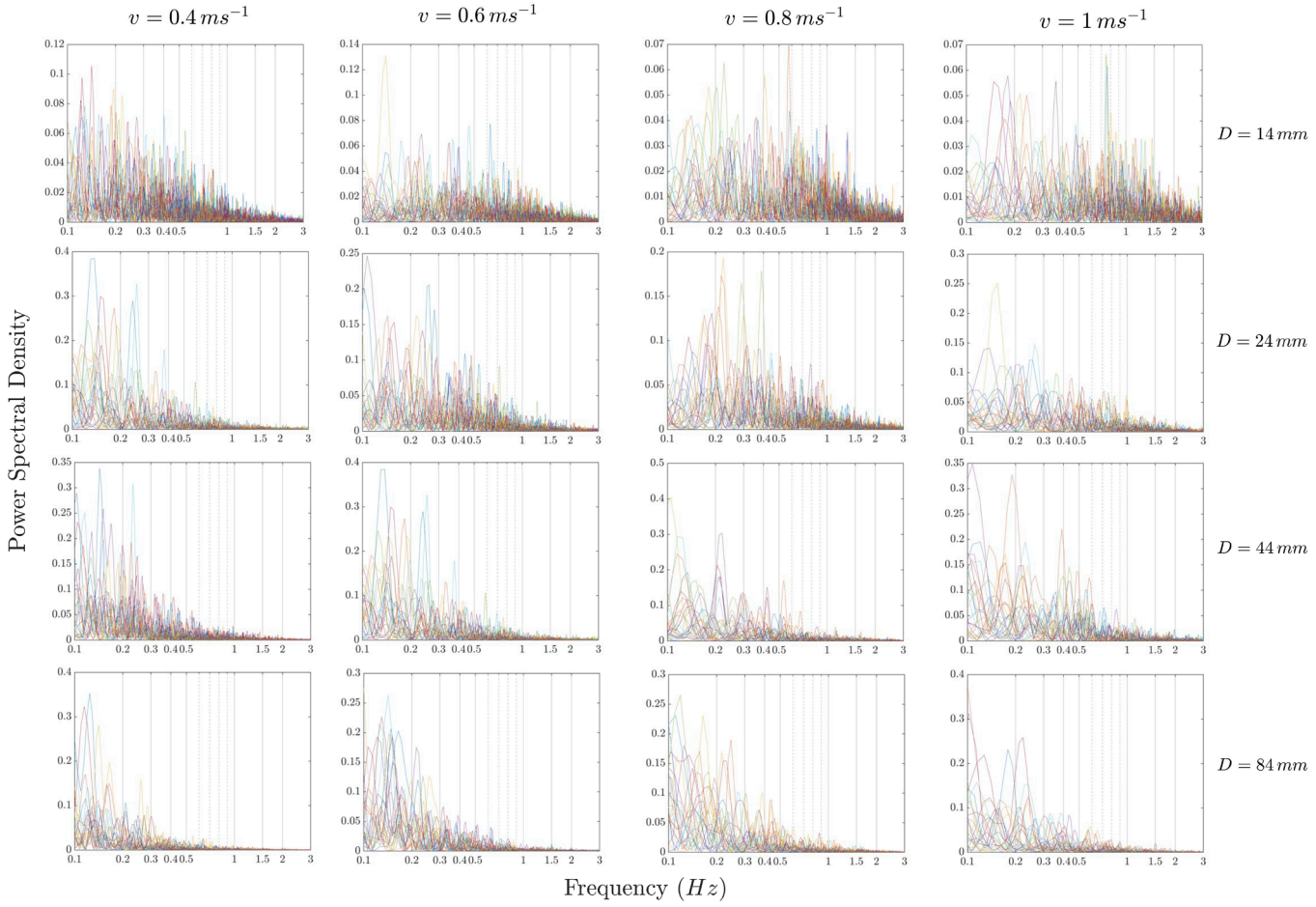

Fig. 4. Lomb-Scargle PSD (Power spectral density) versus frequency in TPBRs of four diameters and circulation velocities.

particles tracked are less constrained. Second, that the frequency of the movement increases with the circulation velocity, as could be expected. This was obscure in Figs. 2 and 3 but is clearly shown here: the frequency of the movement is increased by the circulation velocity but in such a limited and subtle way that it can only be seen in a spectral analysis. Fig. 4 shows that for low circulation velocities (v = 0.4 m s^{-1}), most of the significant amplitude movement takes place between 0.1 and 0.2 Hz meaning that it takes 5–10 s for a particle to move from the surface to the center, and that movement is not complete and only takes place for a fraction of the population out of the 10 particles shown in the plots in Fig. 4. As the circulation velocity increases, the frequency spectrum of the movement widens to 0.5 or even to 1 Hz in some cases. To ascertain the relevance of such mixing frequency, it is useful to use the "characteristic frequency" (ß) proposed by Camacho Rubio et al. (2003). Fernández-Sevilla et al. (2018) demonstrated that when the frequency of the dark/light cycle (ν) equals ß, the integration factor Γ equals 0.62. This factor is a number initially proposed by Terry (1986) that quantifies if the light regime of a microalgal culture corresponds to light integration (Γ = 1), to local growth velocities integration (Γ = 0), or something in between for intermediate values.

$$\Gamma = \frac{P - P_{av}}{P(I_{av}) - P_{av}} \tag{21}$$

where P_{av} represents the local velocity integration, $P(I_{av})$ the response to average light in the PBR (full integration), and P is any other intermediate situation. Since $P_{av} \leq P \leq P(I_{av})$ it follows that $0 \leq \Gamma \leq 1$. The integration factor can be calculated for different situations using the equation proposed by Fernández-Sevilla et al. (2018), as shown in Table 2.

Table 2
Integration factor (Γ) as a function of the adimensional frequency (ν/β) for ideal light/dark cycles under non-saturating irradiance ($I_{av}/\alpha \leq 1$) using the equation proposed by Fernández-Sevilla et al. (2018).

	ν/β				
I_{av}/α	0.1	0.2	0.5	1	2
0.25	0.367	0.571	0.787	0.885	0.940
0.5	0.199	0.367	0.632	0.787	0.885
1	0.100	0.199	0.432	0.632	0.787

For the simulations done in this work, we have a semisaturation situation ($I_{av}/\alpha = 0.5$) as the biomass concentrations in Table 1 have been chosen to result in an average irradiance of approximately I_{av} = 100 μmole photons m^{-2} s^{-1}. The adimensional frequency ν/β used in

Table 3
Characteristic frequencies obtained for several microalgal strains.

β (Hz)	Strain	Source
15.2	*Chlorella vulgaris*	Camacho Rubio et al. (2003) with data from Phillips and Myers (1954)
70.4	*Synechococcus elongatus*	Camacho Rubio et al. (2003) with data from Nedbal et al. (1996)
7.2	*Phaeodactylum tricornutum*	Brindley et al. (2010)
5.7	*Scenedesmus almeriensis*	Brindley et al. (2016)
15.3	*Nannochloropsis oculata*	Fernández-Sevilla et al. (2018)

Table 2 is useful as it allows generalization of the effect of mixing without having to focus on a particular strain, but to be able to ascertain if a given frequency mixing ν is any good to affect the integration factor, it is necessary to know at least an approximation of the value of the characteristic frequency β in microalgae. There are many studies on the effect of flashing light in the literature, but few use the data to obtain β. In Table 3 are summarized some characteristic frequencies of different strains with the corresponding reference. As can be seen, the data show varies from 5 to 70 Hz, although the latter value was obtained using data of Nedbal et al. (1996) that were measured under very high frequencies, and that could have biased the results to some extent.

In this work, we have considered a characteristic frequency $\beta = 5$ Hz, which is on the low side but is feasible. The rationale behind the choice is that microalgal strains with a low β are more productive since they are nearer to a light integration situation and thus should be the strain of choice for the mass production of microalgal biomass.

Therefore, in the conditions of this work ($I_{av}/\alpha = 0.5$ and $\beta = 5$), a mixing frequency of $\nu = 0.5$ Hz corresponding to $\nu/\beta = 0.1$, which the data in Fig. 4 show is possible to bring about an integration factor $\Gamma = 0.199$ which is a modest but significant improvement over the local integration situation. At the higher circulation velocities, some part of the particle population move with a substantial amplitude at frequencies higher than 0.5 Hz, which could lead to integration factors approximating to 0.3 or 0.35 but the main conclusion that can be drawn from Fig. 4, taking into account the information in Tables 1 and 3, is that tubular PBRs are poorly mixed and even in the most favorable conditions a light integration regime is not attained.

Still, the analysis carried out in this section has been done with equations obtained for strict light/dark cycles (as opposed to the continuous variations in real microalgal cultures). Thus, it cannot be ruled out that the smaller, higher frequency movements shown in Fig. 4 can enhance the photosynthetic response, as demonstrated by Brindley et al. (2011). This is analyzed in the next section, where the complete light history of each particle is coupled to a dynamic photosynthesis model to calculate the photosynthetic response.

3.4. Productivity in tubular PBRs is a function of diameter.

In the former sections, it has been shown that the correct way to depict a dense microalgal culture is as a population of microalgae that individually experience a somewhat irregularly changing irradiance pattern usually referred to as "light regime". Although some average values can be calculated for the light regime in dense cultures (e.g., average irradiance), it is clear that the irradiance changes are irregular. Even for a single cell, the trajectories and irradiances vary in amplitude and frequency. Any assimilation of such movements to light/dark cycles needs several arbitrary decisions that remove any generality in the results obtained. Additionally, Brindley et al. (2011) demonstrated mathematically that the "shape" of the movement matters: when a light/dark (a squared wave type) cycle was compared to a continuously varying cycle completely equivalent (same frequency, duty cycle, incident, and average irradiances) by the application of a dynamic photosynthesis model, the results were substantially different.

Therefore, reliably estimating the photosynthetic response in a dense culture requires considering a significant population and using the actual irradiance pattern I(t) coupled to a dynamic photosynthesis model. I(t) arises from the coupling of the irradiance distribution and the cell population trajectories obtained by CFD that in this work has been described by the Lambert-Beer model applied to a cylinder (Eq. (18)). The CFD trajectories x(t) calculated in the former sections have been coupled to the light distribution in the TPBRs of different diameters to obtain the light history I(t) of the 50 particles population. These were then used to calculate the photosynthetic response for the different circulation velocities in order to determine the photosynthetic yield. To calculate the photosynthetic response of the rapidly varying light pattern I(t), the dynamic photosynthesis model of Camacho Rubio et al. (2003) has been used. This model is given as differential equations that take I(t) as input and render a photosynthetic productivity history P(t). The Camacho-Rubio model has been used because of the availability of dynamic parameters for different strains made available by the original work and others (Brindley et al., 2016, 2011; Camacho Rubio et al., 2003; Fernández-Sevilla et al., 2018) and in particular, the convenience of the parameter β "characteristic frequency" that allows an intuitive visualization of the relationship between frequency (ν) and the integration factor (Γ) as previously shown in Table 2.

In Fig. 5 are displayed the results of coupling the light histories of the population with the dynamic photosynthesis model of Camacho Rubio et al. (2003) for a strain with growth parameters $\alpha = 200$ μmole photons m^{-2} s^{-1}, $\beta = 5$ Hz and $\kappa = 0.1$. These are typical values for ubiquitous strains obtained from the reference in Table 2. The response of the model is P/P_{max}, a normalized value that can be easily converted to a specific growth rate (μ), oxygen generation PO_2, or any other. It would be sufficient to multiply P/P_{max} by μ_{max} or $(PO_2)_{max}$. For clarity, only three diameters (14, 44, and 84 mm) and three circulation velocities (0.4, 0.6, and 1 m s^{-1}) are presented. As Fig. 5 shows, the main conclusion drawn from this study is that TPBRs for the culture of microalgae are poorly mixed from the point of view of photosynthetic efficiency. This is true even for a PBR of such a small tube diameter as 14 mm at the highest circulation velocity tested and bearing in mind that the simulation has been done for a strain with a characteristic frequency of $\beta = 5$ Hz, the lowest value registered, and the one that requires the lowest mixing frequency to attain a light integration regime (Table 2).

All the plots in Fig. 5 show two clear zones, a green one of saturated growth and a yellow one of severely limited conditions with a very fast transition in the boundary. This does not mean that these two zones are entirely separated. On the contrary, frequent transitions of fluid elements between these two zones happen so that the culture is mixed with regard to biomass concentration or oxygen saturation, but at the same time, these transitions are slow enough to promote a local photosynthesis rate, as the microalgae have enough time to adapt to local irradiances. Still, in Fig. 5 it is clear that small diameters and higher circulation velocities increase mixing substantially. For D = 14 mm, some trajectories move between the surface and center fast enough to maintain a high photosynthesis rate. Those trajectories appear as single strands that penetrate under the surface at v = 0.4 m s^{-1} and become more abundant at 0.6 and 1 m s^{-1}, reaching virtually any place in the culture volume. Still, most of the culture volume remains highly limited. As the diameters increase to 44 and 84 mm, this effect diminishes. Some trajectories of high productivity penetrate sporadically to depths of little significance but are easy to spot in the corresponding plots of Fig. 5. We have not evaluated the length of these trajectories rigorously, but they correspond to 8–12 mm displacements that become more frequent when the circulation velocity is increased.

These effects can be seen quantitatively in Table 4, where the average integration factors for the 50 particles are shown in all the simulated circumstances. The main conclusion is, again, that tubular PBRs are poorly mixed from the point of view of photosynthetic performance. The best-performing culture corresponds to D = 14 mm and v = 1 m s^{-1}. This is the smallest tube diameter and fastest circulation velocity. In these circumstances, the integration factor Γ reaches a maximum value of 0.1997 $\beta = 5$ Hz and 0.0656 for $\beta = 20$ Hz. This means that even in the most favorable circumstances, the light regime is only 20 % light integration. It is necessary to bear in mind that the conditions in this simulation are stringent for several reasons. On the one hand, no albedo is considered in the light propagation regime, resulting in more intense light gradients difficult to mix for a light integration regime. On the other hand, the operating concentrations chosen are high as these have been chosen assuming maximum productivity ($I_{av} = \alpha/2$). Usually, TPBRs operate at lower biomass concentrations because the integration regime is difficult to attain (remember that, as shown in Table 2, the lower the light saturation, the easier it is to reach a high integration factor).

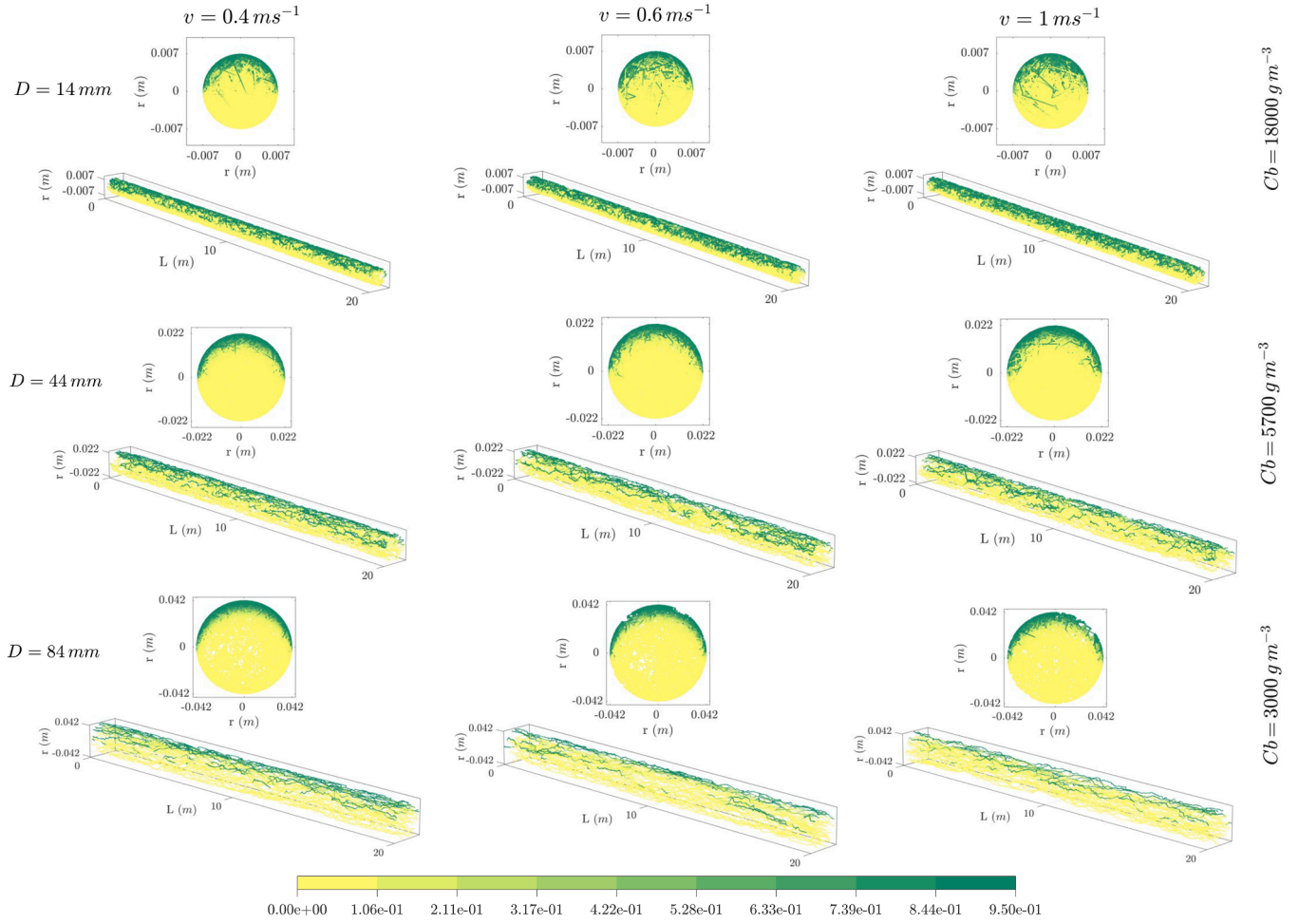

Fig. 5. Adimensional productivities, P/P_{max} calculated for the individual trajectories for different tube diameters and circulation velocities under semisaturating conditions ($I_{av} = \alpha/2$).

Table 4
Integration factors (Γ) obtained for different diameters (D) and circulation velocities (v) for a microalgal strain with growth parameters α = 200 μmol m^{-2} s^{-1}, κ = 0.1 and two different characteristic frequencies (ß). The results are an average of the 50 particles population.

	D (mm)				
v (m/s)	14	24	44	64	84
	β = 5 Hz				
0.4	0.0691	0.0474	0.0315	0.0259	0.0192
0.6	0.1122	0.0970	0.0558	0.0356	0.0266
0.8	0.1616	0.1310	0.0717	0.0529	0.0463
1.0	0.1997	0.1467	0.0851	0.0656	0.0564
	β = 20 Hz				
0.4	0.0227	0.0187	0.0135	0.0115	0.0094
0.6	0.0353	0.0285	0.0199	0.0155	0.0127
0.8	0.0515	0.0382	0.0233	0.0167	0.0159
1.0	0.0656	0.0457	0.0256	0.0219	0.0180
C_b (g m^{-3})	18,000	10,500	5700	3900	3000
I_{av} (μmol photon m^{-2} s^{-1})	99.2	99.2	99.7	100.2	99.2

In Fig. 6, it is analyzed what the information in Table 4 means for the operation of a tubular PBR with an actual microalgal strain. For this, we have chosen the value of μ_{max} = 0.075 h^{-1} found by Sánchez et al. (2008) for *Scenedesmus almeriensis* under an ample variety of circumstances, including outdoor cultures. For this, the specific growth rate corresponding to an integration light regime, $\mu(I_{av})$, is calculated adapting Eq. (16) to use

$$\mu(I_{av}) = \frac{\mu_{max}\cdot I_{av}}{2\cdot\alpha}\cdot\left[\left(1+\kappa+\frac{\alpha}{I_{av}}\right)-\sqrt{\left(1-\kappa-\frac{\alpha}{I_{av}}\right)^2+4\cdot\kappa}\right] \tag{22}$$

Then, the actual specific growth rate taking into account the integrating factor can be calculated by rearranging Eq. (21) to:

$$\mu = \Gamma\cdot(\mu(I_{av})-\mu_{av})+\mu_{av} \tag{23}$$

where Γ is the integration factor in Table 4 and μ_{av} is the average of local specific growth rates calculated adapting Eq. (17) as:

$$\mu_{av} = \frac{\mu_{max}}{\pi\cdot R^2}\int_{-R}^{R}\int_{-\sqrt{R^2-x}}^{\sqrt{R^2-x}}\frac{I(x,y)}{2\cdot\alpha}\cdot\left[\left(1+\kappa+\frac{\alpha}{I(x,y)}\right)-\sqrt{\left(1-\kappa-\frac{\alpha}{I(x,y)}\right)^2+4\cdot\kappa}\right]dydx \tag{24}$$

The volumetric productivity, P_{vol} (g $m^{-3}h^{-1}$) is then obtained by multiplying the net specific growth rate, μ_{net}=μ-m, by the biomass concentration C_b:

$$P_{vol} = C_b\cdot\mu_{net} = C_b\cdot(\mu-m) \tag{25}$$

where m is the specific maintenance rate that in this work, for demonstrative purposes, is given a value of 10% of μ_{max}. Thus m = 0.0075 h^{-1}. On the other hand, the areal productivity, P_{areal}, can be calculated from P_{vol} by multiplying by the occupied area (S) to PBR volume (V) ratio that

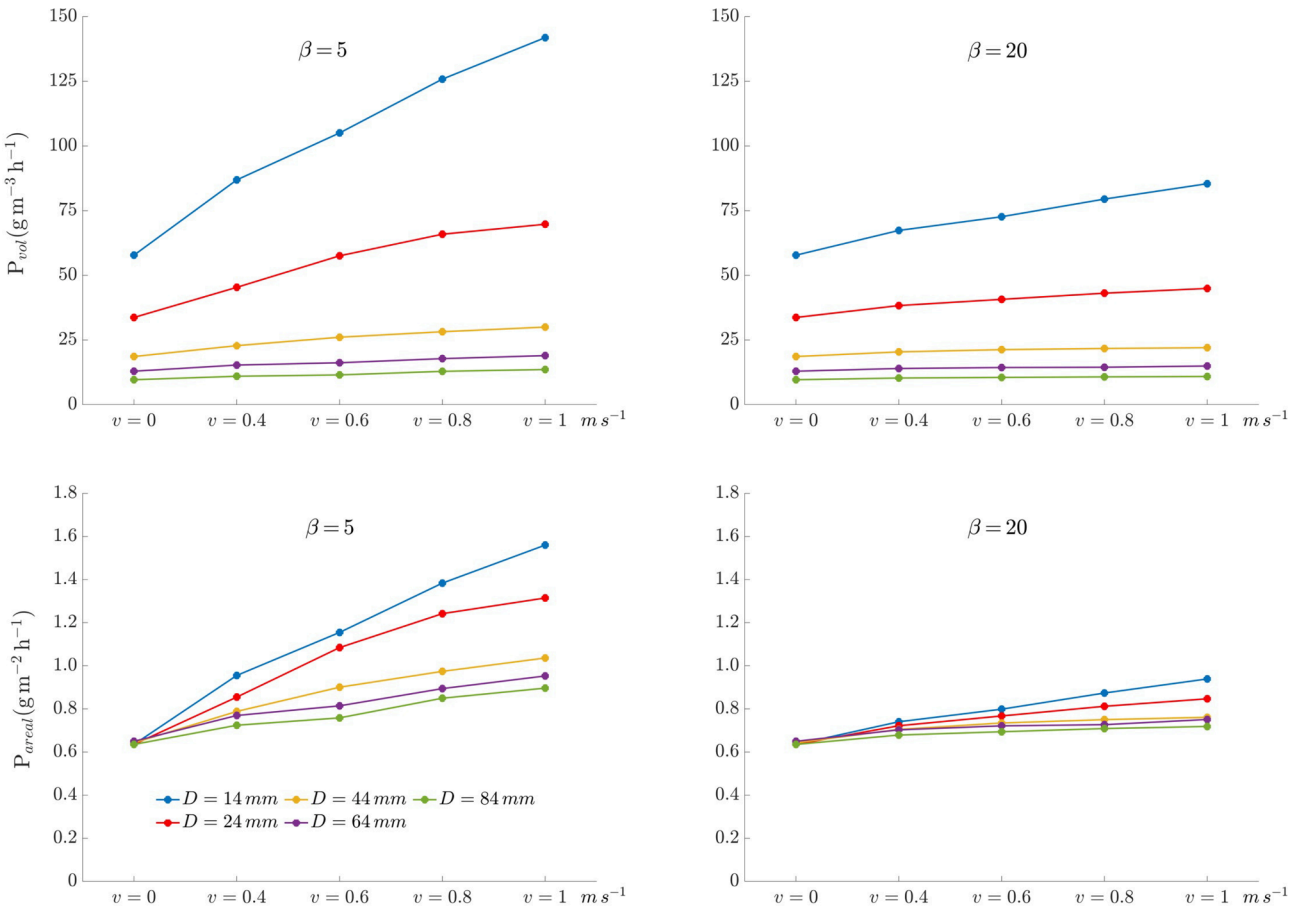

Fig. 6. Volumetric and areal productivity of tubular PBRs for a microalgal strain with $\mu_{max} = 0.075\ h^{-1}$ for the different diameters and circulation velocities tested.

is obtained by simple geometry as:

$$\frac{V}{S} = \frac{\frac{\pi}{4}\cdot D^2 \cdot L}{D \cdot L} = \frac{\pi \cdot D}{4} \tag{26}$$

With V/S in $m^3\ m^{-2}$, P_{areal} is calculated as

$$P_{areal} = P_{vol} \cdot \frac{V}{S} \tag{27}$$

This is shown in Fig. 6, where it is evident that the smaller diameters always result in higher volumetric productivity due to their shorter light path that allows operating at higher biomass concentrations. In spite of the low integration factors obtained (Table 4), the effect of the increasing mixing brought about by higher circulation velocities is significant, especially for the smaller diameters and the strain with a characteristic frequency. Bear in mind that the local integration situation, which strictly never takes place, has been introduced as v = 0 to allow comparison. Still, for D = 84 mm, P_{vol} rises from 11.0 to 13.6 g $m^{-3}h^{-1}$ when v is increased from 0.4 to 1.0 m s^{-1} for ß=5 Hz, which is a 24% increase and thus noticeable although it is not easy to see in the plots. On the other hand, the increase for ß=20 Hz is negligible (from 10.3 to 10.9 g $m^{-3}h^{-1}$). Still, the volumetric productivity in all cases is far from the theoretical maximum that could be attained with perfect mixing, and that is 478.8, 279.3, 152.4, 104.8, and 79.8 g $m^{-3}h^{-1}$ respectively for D = 14, 24, 44, 64, and 84 mm.

With regard to the areal productivity, which is a more realistic value when outdoor, mass cultures are considered, Fig. 6 shows that the effect of an increased mixing brought about by higher circulation velocities is always noticeable for ß=5 Hz although it can be negligible for ß=20 except for the two smallest diameters D = 14 and 24 mm. Despite the low integration factors shown in Table 4, for ß=5 Hz, an increase in v from 0.4 to 1 m s^{-1} in the D = 14 mm PBR increases P_{areal} from 0.96 to 1.56 g $m^{-2}h^{-1}$, which is a 62% increase. For D = 84 mm, the increase is less noticeable but still significant (0.72 to 0.90 g $m^{-2}h^{-1}$, a 25% increase). For ß=20 Hz, the increase in P_{areal} with velocity is 27% for D = 14 mm and only 5% for D = 84 mm.

Thus, circulation velocity has a significant effect enhancing productivity that can be noticed in all the circumstances tested, although it is far from the theoretical maximum of 5.3 g $m^{-2}h^{-1}$ (a value in agreement with the widely accepted maximum of 50–60 g m^{-2} day^{-1}). It is clear from Fig. 6 that devices with a short light path are better mixed and could be an alternative for more productive PBRs.

4. Conclusions

The coupling of CFD to the dynamic photosynthesis model proposed by Camacho Rubio et al. (2003) has allowed us to demonstrate that TPBRs are poorly mixed microalgal culture devices. It has been shown that the frequency of displacements of significant amplitude is under 0.5 Hz, which is small compared to the characteristic frequency (β) of the most tolerant strains, and this leads to low photosynthetic efficiency. There is potential for improvement as the simulation analysis shows that the maximum productivity of 1.56 g $m^{-2}h^{-1}$ could be increased to a theoretical maximum of 5.30 g $m^{-2}h^{-1}$.

CRediT authorship contribution statement

P. Fernández del Olmo: Methodology, Software, Validation, Formal analysis, Investigation, Data curation, Visualization. **F.G. Acién:** Conceptualization, Methodology, Formal analysis, Supervision. **J.M. Fernández-Sevilla:** Conceptualization, Methodology, Formal analysis, Investigation, Resources, Supervision, Project administration, Funding

acquisition.

Declaration of Competing Interest

The authors declare that they have no known competing financial interests or personal relationships that could have appeared to influence the work reported in this paper.

Acknowledgments

This work is supported by the research project PURASOL (CTQ2017-84006-C3-3-R) funded by Ministerio de Economía y Competitividad, Gobierno de España and SABANA project funded by the European Union Framework Programme Horizon 2020 Research and Innovation Programme under the Grant Agreement No. 72787.

References

Assunção, J., Malcata, F.X., 2020. Enclosed "non-conventional" photobioreactors for microalga production: A review. Algal Res. 52, 102107. https://doi.org/10.1016/j.algal.2020.102107.

Belohlav, V., Uggetti, E., García, J., Jirout, T., Kratky, L., Díez-Montero, R., 2021. Assessment of hydrodynamics based on Computational Fluid Dynamics to optimize the operation of hybrid tubular photobioreactors. J. Environ. Chem. Eng. 9 (5), 105768. https://doi.org/10.1016/j.jece:2021.105768.

Bitog, J.P., Lee, I.-B., Lee, C.-G., Kim, K.-S., Hwang, H.-S., Hong, S.-W., Seo, I.-H., Kwon, K.-S., Mostafa, E., 2011. Application of computational fluid dynamics for modeling and designing photobioreactors for microalgae production: A review. Comput. Electron. Agric. 76 (2), 131–147. https://doi.org/10.1016/j.compag.2011.01.015.

Blasius, H., 1913. In: Mitteilungen über Forschungsarbeiten auf dem Gebiete des Ingenieurwesens. Springer Berlin Heidelberg, Berlin, Heidelberg, pp. 1–41. https://doi.org/10.1007/978-3-662-02239-9_1.

Brindley, C., Acién Fernández, F.G., Fernández-Sevilla, J.M., 2010. The oxygen evolution methodology affects photosynthetic rate measurements of microalgae in well-defined light regimes. Biotechnol. Bioeng. 106, 228–237. https://doi.org/10.1002/bit.22676.

Brindley, C., Acién Fernández, F.G., Fernández-Sevilla, J.M., 2011. Analysis of light regime in continuous light distributions in photobioreactors. Bioresour. Technol. 102 (3), 3138–3148. https://doi.org/10.1016/j.biortech.2010.10.088.

Brindley, C., Jiménez-Ruíz, N., Acién, F.G., Fernández-Sevilla, J.M., 2016. Light regime optimization in photobioreactors using a dynamic photosynthesis model. Algal Res 16, 399–408. https://doi.org/10.1016/j.algal.2016.03.033.

Camacho Rubio, F., Camacho, F.G., Sevilla, J.M.F., Chisti, Y., Grima, E.M., 2003. A mechanistic model of photosynthesis in microalgae. Biotechnol. Bioeng. 81 (4), 459–473. https://doi.org/10.1002/(ISSN)1097-029010.1002/bit.v81:410.1002/bit.10492.

Chen, C.-Y., Yeh, K.-L., Aisyah, R., Lee, D.-J., Chang, J.-S., 2011. Cultivation, photobioreactor design and harvesting of microalgae for biodiesel production: A critical review. Bioresour. Technol. 102 (1), 71–81. https://doi.org/10.1016/j.biortech.2010.06.159.

Eilers, P.H.C., Peeters, J.C.H., 1988. A model for the relationship between light intensity and the rate of photosynthesis in phytoplankton. Ecol. Modell. 42 (3-4), 199–215. https://doi.org/10.1016/0304-3800(88)90057-9.

Emerson, R., Arnold, W., 1932. The photochemical reaction in photosynthesis. J. Gen. Physiol. 16 (2), 191–205. https://doi.org/10.1085/jgp.16.2.191.

Fernández-Sevilla, J.M., Brindley, C., Jiménez-Ruíz, N., Acién, F.G., 2018. A simple equation to quantify the effect of frequency of light/dark cycles on the photosynthetic response of microalgae under intermittent light. Algal Res 35, 479–487. https://doi.org/10.1016/j.algal.2018.09.026.

Fernández del Olmo, P., Acién, F.G., Fernández-Sevilla, J.M., 2021. Analysis of productivity in raceway photobioreactor using computational fluid dynamics particle tracking coupled to a dynamic photosynthesis model. Bioresour. Technol. 334, 125226. https://doi.org/10.1016/j.biortech.2021.125226.

Gao, X.i., Kong, B.o., Vigil, R.D., 2017. Comprehensive computational model for combining fluid hydrodynamics, light transport and biomass growth in a Taylor vortex algal photobioreactor: Lagrangian approach. Bioresour. Technol. 224, 523–530. https://doi.org/10.1016/j.biortech.2016.10.080.

Gómez-Pérez, C.A., Espinosa, J., Montenegro Ruiz, L.C., van Boxtel, A.J.B., 2015. CFD simulation for reduced energy costs in tubular photobioreactors using wall turbulence promoters. Algal Res 12, 1–9. https://doi.org/10.1016/j.algal.2015.07.011.

Gómez-Pérez, C.A., Espinosa Oviedo, J.J., Montenegro Ruiz, L.C., van Boxtel, A.J.B., 2017. Twisted tubular photobioreactor fluid dynamics evaluation for energy consumption minimization. Algal Res. 27, 65–72. https://doi.org/10.1016/j.algal.2017.08.019.

Lomb, N.R., 1976. Least-squares frequency analysis of unequally spaced data. Astrophys. Space Sci. 39 (2), 447–462. https://doi.org/10.1007/BF00648343.

Mata, T.M., Martins, A.A., Caetano, N.S., 2010. Microalgae for biodiesel production and other applications: A review. Renew. Sustain. Energy Rev. 14 (1), 217–232. https://doi.org/10.1016/j.rser.2009.07.020.

Molina, E., Fernández, J., Acién, F.G., Chisti, Y., 2001. Tubular photobioreactor design for algal cultures. J. Biotechnol. 92 (2), 113–131. https://doi.org/10.1016/S0168-1656(01)00353-4.

Molina Grima, E., Camacho, F.G., Pérez, J.A.S., Sevilla, J.M.F., Fernández, F.G.A., Gómez, A.C., 1994. A mathematical model of microalgal growth in light-limited chemostat culture. J. Chem. Technol. Biotechnol. 61 (2), 167–173. https://doi.org/10.1002/(ISSN)1097-466010.1002/jctb.v61:210.1002/jctb.280610212.

Molina Grima, E., García Camacho, F., Sánchez Pérez, J.A., Acién Fernández, F.G., Fernández Sevilla, J.M., 1997. Evaluation of photosynthetic efficiency in microalgal cultures using averaged irradiance. Enzyme Microb. Technol. 21 (5), 375–381. https://doi.org/10.1016/S0141-0229(97)00012-4.

Nedbal, L., Tichý, V., Xiong, F., Grobbelaar, J.U., 1996. Microscopic green algae and cyanobacteria in high-frequency intermittent light. J. Appl. Phycol. 8 (4-5), 325–333. https://doi.org/10.1007/BF02178575.

Nelson, D.L., Cox, M.M., 2017. Lehninger Principles of Biochemistry 7th. W.H, Freeman and Company.

Nikolaou, A., Booth, P., Gordon, F., Yang, J., Matar, O., Chachuat, B., 2016. Multi-Physics Modeling of Light-Limited Microalgae Growth in Raceway Ponds. IFAC-PapersOnLine 49 (26), 324–329. https://doi.org/10.1016/j.ifacol.2016.12.147.

Patankar, S.V., 1980. Numerical heat transfer and fluid, flow. Ed. Hemisph. Publ. Corp, New York.

Perner-Nochta, I., Posten, C., 2007. Simulations of light intensity variation in photobioreactors. J. Biotechnol. 131 (3), 276–285. https://doi.org/10.1016/j.jbiotec.2007.05.024.

Phillips, J.N., Myers, J., 1954. Growth Rate of Chlorella in Flashing Light. Plant Physiol 29 (2), 152–161. https://doi.org/10.1104/pp.29.2.152.

Pires, J.C.M., Alvim-Ferraz, M.C.M., Martins, F.G., 2017. Photobioreactor design for microalgae production through computational fluid dynamics: A review. Renew. Sustain. Energy Rev. 79, 248–254. https://doi.org/10.1016/j.rser.2017.05.064.

Posten, C., 2009. Design principles of photo-bioreactors for cultivation of microalgae. Eng. Life Sci. 9 (3), 165–177. https://doi.org/10.1002/elsc.v9:310.1002/elsc.200900003.

Prussi, M., Buffi, M., Casini, D., Chiaramonti, D., Martelli, F., Carnevale, M., Tredici, M. R., Rodolfi, L., 2014. Experimental and numerical investigations of mixing in raceway ponds for algae cultivation. Biomass and Bioenergy 67, 390–400. https://doi.org/10.1016/j.biombioe.2014.05.024.

Pulz, O., 2001. Photobioreactors: Production systems for phototrophic microorganisms. Appl. Microbiol. Biotechnol. https://doi.org/10.1007/s002530100702.

Qin, C., Wu, J., 2019. Influence of successive and independent arrangement of Kenics mixer units on light/dark cycle and energy consumption in a tubular microalgae photobioreactor. Algal Res. 37, 17–29. https://doi.org/10.1016/j.algal.2018.09.020.

Richmond, A., 2004. Principles for attaining maximal microalgal productivity in photobioreactors: An overview, in: Hydrobiologia. 10.1023/B:HYDR.0000020365.06145.36.

Richmond, A., Hu, Q., 2013. Handbook of Microalgal Culture: Applied Phycology and Biotechnology: Second Edition, Handbook of Microalgal Culture: Applied Phycology and Biotechnology: Second Edition. 10.1002/9781118567166.

Sánchez, J.F., Fernández-Sevilla, J.M., Acién, F.G., Cerón, M.C., Pérez-Parra, J., Molina-Grima, E., 2008. Biomass and lutein productivity of Scenedesmus almeriensis: Influence of irradiance, dilution rate and temperature. Appl. Microbiol. Biotechnol. 79 (5), 719–729. https://doi.org/10.1007/s00253-008-1494-2.

Spolaore, P., Joannis-Cassan, C., Duran, E., Isambert, A., 2006. Commercial applications of microalgae. J. Biosci. Bioeng. 101 (2), 87–96. https://doi.org/10.1263/jbb.101.87.

Suparmaniam, U., Lam, M.K., Uemura, Y., Lim, J.W., Lee, K.T., Shuit, S.H., 2019. Insights into the microalgae cultivation technology and harvesting process for biofuel production: A review. Renew. Sustain. Energy Rev. 115, 109361. https://doi.org/10.1016/j.rser.2019.109361.

Terry, K.L., 1986. Photosynthesis in modulated light: Quantitative dependence of photosynthetic enhancement on flashing rate. Biotechnol. Bioeng. 28 (7), 988–995. https://doi.org/10.1002/(ISSN)1097-029010.1002/bit.v28:710.1002/bit.260280709.

Ugwu, C.U., Aoyagi, H., Uchiyama, H., 2008. Photobioreactors for mass cultivation of algae. Bioresour. Technol. 99 (10), 4021–4028. https://doi.org/10.1016/j.biortech.2007.01.046.

Veenman, M.P.B., 2004. Statistical analysis of turbulent pipe flow: a numerical approach. Eindhoven University of Technology, Eindhoven, The Netherlands http://alexandria.tue.nl/extra2/200411530.pdf.

Walpot, R.J.E., van der Geld, C.W.M., Kuerten, J.G.M., 2007. Determination of the coefficients of Langevin models for inhomogeneous turbulent flows by three-dimensional particle tracking velocimetry and direct numerical simulation. Phys. Fluids 19 (4), 045102. https://doi.org/10.1063/1.2717688.

Wen, Z.-Y., Chen, F., 2003. Heterotrophic production of eicosapentaenoic acid by microalgae. Biotechnol. Adv. 21 (4), 273–294. https://doi.org/10.1016/S0734-9750(03)00051-X.